



Cite this: *New J. Chem.*, 2021, 45, 431

# Monomeric vanadium oxide: a very efficient species for promoting aerobic oxidative dehydrogenation of N-heterocycles†

Zhenbing Xie,<sup>ab</sup> Bingfeng Chen,<sup>id</sup> \*<sup>a</sup> Lirong Zheng,<sup>id</sup> <sup>c</sup> Fangfang Peng,<sup>a</sup> Huizhen Liu<sup>id</sup> \*<sup>ab</sup> and Buxing Han<sup>id</sup> \*<sup>ab</sup>

Monomeric active species are very interesting in heterogeneous catalysis. In this work, we proposed a method to prepare  $\text{VO}_x\text{-NbO}_y/\text{C}$  catalysts, which involve the one-pot hydrothermal synthesis of inorganic/organic hybrid materials containing V/Nb followed by thermal treatment under a reducing atmosphere. The prepared catalysts were characterized using different techniques, such as high-angle annular dark-field scanning transmission electron microscopy and X-ray absorption fine structure spectroscopy. It was shown that monomeric  $\text{VO}_x$  species were dispersed homogeneously in the catalysts. The  $\text{VO}_x\text{-NbO}_y/\text{C}$  catalysts displayed high performance in the aerobic oxidative dehydrogenation of N-heterocycles to aromatic heterocycles. It was demonstrated that the selectivity of reaction over the catalyst with a very small amount of V (0.07 wt%) was much higher than that over the  $\text{NbO}_y/\text{C}$ , and the catalyst also exhibited excellent stability in the reaction. The detailed study indicated that monomeric  $\text{VO}_2$  species were the most effective for promoting the reaction.

Received 23rd September 2020,  
 Accepted 24th November 2020

DOI: 10.1039/d0nj04708b

rs.c.li/njc

## Introduction

Vanadium metal is very attractive in catalysts because it is an earth-abundant metallic element and has a low toxicity compared to most other heavy metals. Vanadium-based catalysts have been widely used in chemical, petroleum and environmental industries, such as industrial production of  $\text{H}_2\text{SO}_4$ ,<sup>1</sup> maleic anhydride<sup>2</sup> and phthalic anhydride,<sup>3</sup> and selective catalytic reduction (SCR) of harmful  $\text{NO}_x$ .<sup>4,5</sup> Vanadium-based catalysts, such as vanadium silicate zeolites<sup>6</sup> and divanadium-substituted phospho-tungstate,<sup>7</sup> have been reported in the catalytic hydroxylation of arenes to phenols. Moreover, supported vanadium oxides catalysts have also been used in the catalytic dehydrogenation of light alkanes.<sup>8</sup> The catalytic performances of supported vanadium oxide catalysts are closely correlated with the dispersion state of active sites, in which the reported vanadium species exist as monomeric  $\text{VO}_x$  species,

polymeric surface  $\text{VO}_4$  sites or  $\text{V}_2\text{O}_5$  nanoparticles.<sup>9</sup> It has been reported that the isolated  $\text{VO}_x$  species exhibited higher catalytic activity and selectivity in the catalytic dehydrogenation of propane compared with their oligomerized counterparts.<sup>10</sup> Conventional methods like impregnation and anchoring always result in a broad variety of  $\text{V}_x\text{O}_y$  species. However, other catalyst synthesis methods, such as flame spray pyrolysis<sup>11</sup> and atomic layer deposition,<sup>12</sup> were restricted by the complicated procedures and high cost of volatile molecular metal precursors. Hence, developing highly dispersed vanadium-based catalysts using a feasible procedure is highly desirable for their applications.

During the last decade, much attention has been paid to the study of single-atom catalysts (SAC), which exhibit distinctive performance and achieve the highest utilization efficiency of metal atoms.<sup>13</sup> Recently, Farha and co-workers reported the synthesis of a single-atom-based organo-vanadium species incorporated in MOFs, which could catalyse the selective oxidation of alcohol.<sup>14</sup> However, the poor thermal stability of MOF materials hinders their application. Owing to the high surface free energy of SAC,<sup>15</sup> the atomic dispersed metal sites are generally stabilized by the N atoms with an empty orbital on the surface of nitrogen doped carbon materials,<sup>16</sup> or defects of metal oxides,<sup>17</sup> metal sulfides,<sup>18</sup> metal nitrides<sup>19</sup> and metal-organic frameworks (MOFs).<sup>20</sup>

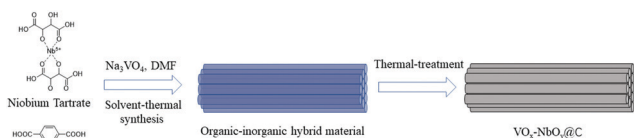
The catalytic dehydrogenation of N-heterocycles is referred to as an important route of synthesis of the corresponding aromatic heterocycles, which are common intermediates in

<sup>a</sup> Beijing National Laboratory for Molecular Sciences, CAS Key Laboratory of Colloidal and Interface and Thermodynamics, Institute of Chemistry, Chinese Academy of Sciences, Beijing, 100190, P. R. China. E-mail: chenbf@iccas.ac.cn, liuhz@iccas.ac.cn, hanbx@iccas.ac.cn

<sup>b</sup> School of Chemistry and Chemical Engineering, University of Chinese Academy of Sciences, Beijing, 100049, P. R. China

<sup>c</sup> Institute of High Energy Physics, Chinese Academy of Sciences, Beijing, 100049, P. R. China

† Electronic supplementary information (ESI) available. See DOI: 10.1039/d0nj04708b



**Scheme 1** The schematic illustration of the preparation procedure for  $\text{VO}_x\text{-NbO}_y\text{@C}$  materials.

pharmaceutical and biological molecules.<sup>21</sup> Several supported metal catalysts, such as Rh,<sup>22</sup> Co,<sup>23</sup> Fe<sup>24</sup> or Ni<sup>25</sup> catalysts, have been reported in the non-oxidative dehydrogenation of N-heterocycles. Although homogeneous oxovanadium (V) catalysts have been applied in the oxidative dehydrogenation of N-heterocycles,<sup>26</sup> heterogeneous catalysts are preferred owing to their heterogeneity and easy separation from the reaction mixture. Although  $\text{V}_2\text{O}_5$  has been used to catalyse the dehydroaromatization, the catalyst dosage was greater than the stoichiometric value.<sup>27</sup> Niobium-based catalytic materials have been used in several selective oxidations and acid-catalysed reactions.<sup>28</sup> Although supported  $\text{V}_2\text{O}_5/\text{Nb}_2\text{O}_5$  catalysts have been reported in the oxidative dehydrogenation of ethane and propane,<sup>29,30</sup> mononuclear vanadium catalysts have not been reported previously for the oxidative dehydrogenation of N-heterocycles.

Herein, we developed a novel method for the fabrication of  $\text{VO}_x\text{-NbO}_y\text{@C}$  catalysts, in which monomeric  $\text{VO}_x$  species were dispersed uniformly in the catalytic materials. Owing to the excellent coordination ability of tartaric acid, the natural carboxylic acid was used to control the dispersion of the vanadium species, which is different from the conventional methods used for vanadium-based catalysts. In this route, the inorganic/organic hybrid materials containing V/Nb were initially prepared *via* the one-pot hydrothermal synthesis. Then the materials were made to undergo thermal treatment under a reducing atmosphere to obtain  $\text{VO}_x\text{-NbO}_y\text{@C-T}$  catalysts, in which *T* represents the temperature of heat-treatment. It was found that the catalyst was very efficient and stable for catalyzing the oxidative dehydrogenation of N-heterocycles (Scheme 1).

## Experimental

### Materials

Niobium pentoxide (99.9%), trisodium tetraoxovanadate dodecahydrate ( $\text{Na}_3\text{VO}_4 \cdot 12\text{H}_2\text{O}$ , 99%), HF ( $\geq 40.0\%$ ), ammonium hydroxide (25–28%), L-(+)-tartaric acid (99.5%), *N,N*-dimethylformamide (DMF, AR), methanol (AR), dimethyl sulfoxide (DMSO, AR), dioxane (AR), *t*-BuOH (AR), and  $\text{CH}_3\text{CN}$  (AR) were purchased from Sinopharm Chemical Reagent. Benzotrile (AR), chlorobenzene (AR) and 1,3,5-trimethylbenzene (AR) were provided by Acros. Terephthalic acid (99%), 1,2,3,4-tetrahydroquinoline (99%), 7-nitro-1,2,3,4-tetrahydroquinoline (98%), 6-methyl-1,2,3,4-tetrahydroquinoline (98%), 6-bromo-1,2,3,4-tetrahydroquinoline (98%), indoline (99%), 6-nitroindoline (98%), 1,2,3,4-tetrahydroisoquinoline (98%), and 1,2,3,4-tetrahydroquinoxaline (98%) were obtained from Alfa Aesar.

### Catalyst preparation

**Preparation of niobium tartrate.** The niobium tartrate solution was prepared from niobium oxide, as reported by P. Pramanik.<sup>31</sup> Niobium oxide (5.31 g) was dissolved in hydrofluoric acid (40%, 18 mL) in a plastic bottle. After being stirred at 80 °C overnight, the residual solids were filtered. The resulting niobium-fluoride complex solution was precipitated by the addition of an aqueous solution of dilute ammonia (ammonia solution :  $\text{H}_2\text{O}$  = 1 : 2 (v/v), 80 mL). The obtained white precipitate of  $\text{Nb}_2\text{O}_5 \cdot n\text{H}_2\text{O}$  was filtered and washed with 5% ammonia solution to remove fluoride ions. Finally, the solid was added into the aqueous tartaric acid solution (320 mL, 0.25 mol  $\text{L}^{-1}$ ). After stirring for a few minutes, aqueous niobium tartrate solution was obtained.

**Preparation of organic-inorganic hybrid material containing niobium.** A certain amount of niobium tartrate solution (20 mL) was mixed with terephthalic acid (1.038 g) and DMF (30 mL).

Terephthalic acid was used as a ligand for preparing the organic-inorganic hybrid material, analogous to the metal-organic frameworks. DMF was used to enhance the solubility of terephthalic acid in the aqueous solution. After sonication for 1.0 h, the clear solution was transferred into hydrothermal reaction vessels. After solvothermal treatment at 220 °C for 8 h, the hybrid material was obtained. In order to remove residual terephthalic acid, the obtained white powder was made to undergo Soxhlet extraction with MeOH and was washed with DMF. After being dried overnight at 333 K under vacuum,  $\text{NbO}_y\text{@C}$  was obtained by thermal treatment at 800 °C under  $\text{H}_2/\text{Ar}$  ( $\text{H}_2$ : 10%, v/v).

**Preparation of vanadium-based catalysts.** The vanadium-based materials were synthesized using a similar solvothermal method. A certain amount of  $\text{Na}_3\text{VO}_4 \cdot 12\text{H}_2\text{O}$  (50 mg) was added to the above-mentioned niobium tartrate solution (20 mL). The solution was mixed with terephthalic acid (1.038 g) and DMF (30 mL). Terephthalic acid was used as a ligand for preparing the organic-inorganic hybrid material. DMF was used to enhance the solubility of terephthalic acid in the aqueous solution. After ultrasonically dissolving the ligand, the mixed solution was made to undergo solvothermal treatment at 220 °C for 8 hours. The obtained solid was treated by Soxhlet extraction with MeOH to remove redundant ligand, and was dried in a vacuum oven at 333 K overnight. The single-atom vanadium-based catalysts were obtained *via* thermal treatment under  $\text{H}_2/\text{Ar}$  ( $\text{H}_2$ : 10%, v/v), which was performed at certain temperatures (600, 700 and 800 °C) for 1.5 h (2 °C  $\text{min}^{-1}$ ). The catalysts were denoted as  $\text{VO}_x\text{-NbO}_y\text{@C-T}$  ( $T$  = 600, 700, 800, and 900), in which *T* represents the thermal-treatment temperature.

### Catalytic reaction

Oxidative dehydrogenation of N-heterocycles was performed in a 12 mL stainless autoclave equipped with a pressure gauge, a magnetic stirrer, and an electric temperature controller. The catalyst (50.0 mg), the solvent (2.0 mL) and N-containing compounds (0.5 mmol) were introduced into the reactor. The sealed autoclave was flushed with  $\text{O}_2$  three times, and pressurized with  $\text{O}_2$  to 0.5 MPa. After the designated temperature was reached, the reaction mixture was stirred at a rate of 800 rpm to

start the reaction. At the end of the reaction, the autoclave was cooled to ambient temperature in water and slowly depressurized. Conversion and product composition were analyzed by GC and GC-MS. Chlorobenzene was used as the internal standard. GC was performed on a GC-2014 (SHIMADZU) equipped with a high-temperature capillary column (MXT-1, 30 m, 0.25 mm I.D.) and an FID detector. GC-MS was performed on a GCT Premier/Waters instrument equipped with a capillary column (DB-5MS/J&W Scientific, 30 m, 0.25 mm I.D.). For NMR analysis, the crude reaction mixture was washed with H<sub>2</sub>O several times to remove DMSO and the aqueous phase was extracted with CH<sub>2</sub>Cl<sub>2</sub>. After drying with Na<sub>2</sub>SO<sub>4</sub> and evaporating under vacuum, the crude products were purified by column chromatography [hexane/ethyl acetate] to get the corresponding product yields.

### Catalyst characterization

XRD patterns were obtained on a Rigaku D/Max-2500 X-ray diffractometer using Cu K $\alpha$  radiation. The elemental analysis was performed using a PerkinElmer Optima 2000 OV inductively coupled plasma-optical emission spectroscope (ICP-OES). Transmission electron microscopy (TEM) was performed on a JEOL 2010 TEM equipped with an attachment for local energy dispersion analysis (EDX). The accelerating voltage was 200 kV, and the spot size was 1 nm. X-Ray photoelectron spectra (XPS) were recorded on a Thermo Scientific ESCA Lab 250 Xi using 200 W mono-chromated Al K $\alpha$  radiation (1486.6 eV). The binding energies were referenced to the C 1s line at 284.8 eV from adventitious carbon. Nitrogen adsorption-desorption analysis was carried out at 77 K on a NOVA 2200e adsorption analyser. Before the adsorption analysis, the samples were degassed under vacuum at 300 °C in the port of the adsorption analyser. <sup>1</sup>H NMR and <sup>13</sup>C NMR spectra were recorded using a Bruker Ultra-Shield 400 MHz spectrometer (<sup>1</sup>H = 400 MHz), with CDCl<sub>3</sub> as the solvent unless otherwise indicated. Tetramethyl-silane (TMS) was used as an internal standard. Raman spectra were recorded on a LabRAM HR Raman microscope equipped with a 532 nm laser source and a 100 $\times$  objective lens. The sample powders were sandwiched between two glass slides before the test.

The X-ray absorption spectra (XAS) including the X-ray absorption near-edge structure (XANES) and extended X-ray absorption fine structure (EXAFS) of the samples at the V K-edge were collected at the 1W1B station in the Beijing Synchrotron Radiation Facility (BSRF), China. The electron storage ring of BSRF was operated at 23 keV. The spectra were recorded in the solid-state detectors for the V K-edge by using an Si(311) double-crystal monochromator, respectively. The Athena software package was used to analyse the data. Theoretical XANES spectra were calculated by using the FEFF8.2 code.

## Results and discussion

Firstly, the niobium-based inorganic/organic hybrid materials were synthesized using a facile hydrothermal process using niobium tartrate, Na<sub>3</sub>VO<sub>4</sub> and terephthalic acid with DMF as

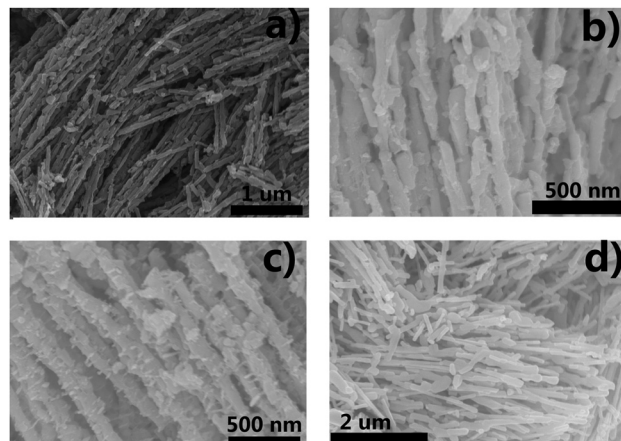
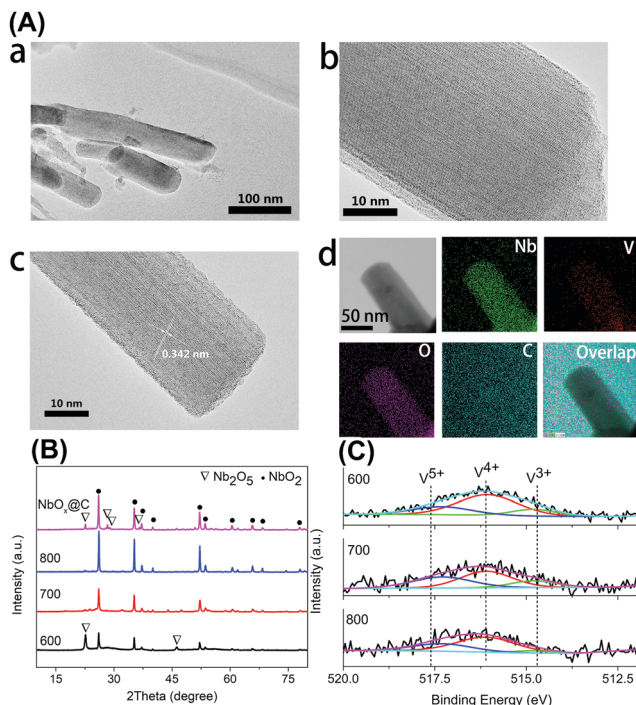


Fig. 1 SEM images of the VO<sub>x</sub>-NbO<sub>y</sub>@C-800 material (a)–(c) and the NbO<sub>y</sub>@C-800 material (d).

solvent. After Soxhlet extraction with MeOH to remove residual terephthalic acid, the hybrid materials were subjected to high temperature under a H<sub>2</sub>/Ar (H<sub>2</sub>: 10%, v/v) atmosphere, and the obtained VO<sub>x</sub>-NbO<sub>y</sub>@C material had a rod-like morphology (Fig. 1a–c). In the absence of Na<sub>3</sub>VO<sub>4</sub>, similar nanorod-structured materials (simplified as NbO<sub>E</sub>@C) were also synthesized (Fig. 1d and Fig. S1, ESI<sup>†</sup>). The excessive tartrates provided the coordination environments for complexing the vanadium and niobium precursors during the hydrothermal procedure. Owing to the excellent coordination ability of tartaric acid, this natural carboxylic acid was helpful for uniform dispersion of VO<sub>x</sub> and NbO<sub>y</sub> species in the hybrid materials.

The Raman spectra of VO<sub>x</sub>-NbO<sub>y</sub>@C showed only two bands corresponding to the G (1580 cm<sup>-1</sup>) and D (1360 cm<sup>-1</sup>) bands, which are the characteristic peaks of carbon materials,<sup>32</sup> but no peak derived from VO<sub>x</sub> species was detected (Fig. S2, ESI<sup>†</sup>). The carbonaceous species, derived from the carbonization of the residual terephthalic acid and tartrate, acted as a support for monomeric VO<sub>x</sub> species and NbO<sub>y</sub> oxides. Besides, they also provided good porosity of the catalysts. ICP analysis revealed that the content of V in VO<sub>x</sub>-NbO<sub>y</sub>@C-800 was 0.07 wt%. As shown in the high-resolution TEM images (Fig. 2b and c), the lattice space of the VO<sub>x</sub>-NbO<sub>y</sub>@C-800 nanorods is 0.342 nm, corresponding to the [400] planes of NbO<sub>2</sub>.<sup>33</sup> Before thermal treatment, both NbO<sub>y</sub>@C and VO<sub>x</sub>-NbO<sub>y</sub>@C showed a pseudo-hexagonal Nb<sub>2</sub>O<sub>5</sub> phase (JCPDS no. 28-0317) (Fig. S3, ESI<sup>†</sup>). After thermal-treatment at 600 °C under a reducing atmosphere, both NbO<sub>2</sub> and Nb<sub>2</sub>O<sub>5</sub> phases were detected in VO<sub>x</sub>-NbO<sub>y</sub>@C (Fig. 2B). Further increasing the temperature resulted in transition from the Nb<sub>2</sub>O<sub>5</sub> phase to the tetragonal NbO<sub>2</sub> phase, which was confirmed by XRD analysis. However, no crystal phases related to vanadium species were detected by X-ray diffraction analysis (Fig. S4, ESI<sup>†</sup>), which indicated that either no crystal vanadium oxide phase was formed in the VO<sub>x</sub>-NbO<sub>y</sub>@C catalysts or the amount of vanadium oxides was too low to be detected using the XRD method. Moreover, high-angle annular dark-field scan TEM (HAADF-STEM) images and corresponding elemental mapping of VO<sub>x</sub>-NbO<sub>y</sub>@C-800 showed the homogeneous



**Fig. 2** The characterization of the  $\text{VO}_x\text{-NbO}_y\text{@C}$  catalyst: (A) TEM images of  $\text{VO}_x\text{-NbO}_y\text{@C-800}$ : (a) low-resolution TEM images; (b) and (c) high-resolution TEM images; (d) EDS mapping; (B) PXRD patterns of  $\text{NbO}_y\text{@C}$  and  $\text{VO}_x\text{-NbO}_y\text{@C}$  undergoing thermal treatment at different temperatures; (C) XPS curve-fitting of the V  $2p_{3/2}$  photoelectronic peak of  $\text{VO}_x\text{-NbO}_y\text{@C}$  catalysts after thermal treatment at different temperatures.

distribution of V, Nb, O and C elements throughout the materials (Fig. 2A).

X-Ray photoelectron spectroscopy (XPS) was performed to characterize the surface compositions of catalytic materials. The high-resolution of the V  $2p_{3/2}$  spectra can be deconvoluted into three peaks located at 517.6 eV, 516.1 eV and 514.7 eV (Fig. 2C), which can be assigned to the  $\text{V}^{5+}$ ,  $\text{V}^{4+}$  and  $\text{V}^{3+}$  species, respectively.<sup>34</sup> The V  $2p_{3/2}$  spectra also demonstrate that the main composition of  $\text{VO}_x\text{-NbO}_y\text{@C}$  was the  $\text{V}^{4+}$  species. The Nb 3d spectra showed three peaks at the binding energies of 207.4 eV ( $3d_{5/2}$ ), 206.8 eV ( $3d_{5/2}$ ) and 205.8 eV ( $3d_{5/2}$ ) (Fig. S5, ESI<sup>†</sup>), which can be ascribed to  $\text{Nb}^{5+}$ ,  $\text{Nb}^{4+}$  and  $\text{Nb}^{3+}$  species, respectively.<sup>35</sup> Although the content of low valence Nb species increased with the thermal-treatment temperature, the  $\text{Nb}^{5+}$  species existed as the main component in these materials (Table S1, ESI<sup>†</sup>). From  $\text{N}_2$  adsorption-desorption isotherms (Fig. S6, ESI<sup>†</sup>), the BET surface area of the  $\text{VO}_x\text{-NbO}_y\text{@C-800}$  was found to be  $59.9 \text{ m}^2 \text{ g}^{-1}$ , and the BJH average pore diameter was centred at 3.9 nm.

The chemical oxidation state and local coordinate structures of the V species in the  $\text{VO}_x\text{-NbO}_y\text{@C}$  were further studied by X-ray absorption near-edge structure (XANES) and extended X-ray absorption fine structure (EXAFS) spectroscopy at the V K-edge. As shown in the XANES spectra (Fig. 3a),  $\text{VO}_x\text{-NbO}_y\text{@C-600}$  showed a strong pre-edge peak comparable to that of  $\text{VO}_2$ , which can be assigned to the so-called  $1s\text{-}3d$  transition originated mainly from the mixing of  $2p$  orbitals of the oxygen anions with

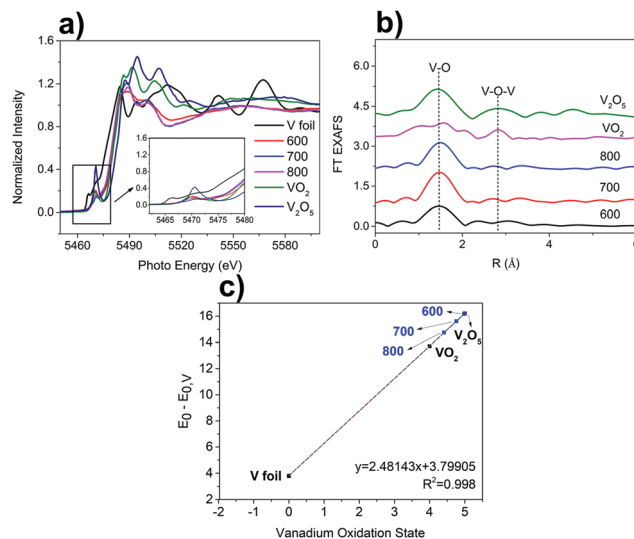


**Fig. 3** (a) V K-edge XANES spectra (the inset shows a magnified view of the pre-edge peaks) and (b) Fourier transformed V K-edge EXAFS spectra of the  $\text{VO}_x\text{-NbO}_y\text{@C}$  catalysts and the reference compounds; (c) the plot of the relative edge position to  $E_0$  (5465 eV) vs. the formal vanadium oxidation state, with the measurements for the  $\text{VO}_x\text{-NbO}_y\text{@C}$  samples indicated on the calibration curve.

$3d$  orbitals of the vanadium atoms.<sup>36</sup> After thermal treatment at higher temperatures, the intensity of the pre-edge peak decreased, and the binding energy at adsorption edge shifted to lower energy (Fig. 3a and Fig. S7, ESI<sup>†</sup>). These results indicate that the vanadium species was reduced to lower valence under high temperature treatment.<sup>37</sup> The position of the white line peak of  $\text{VO}_x\text{-NbO}_y\text{@C}$  was close to that of  $\text{VO}_2$ , indicating that the average valence state of V in the hybrid was approximately  $\text{V}^{4+}$ . Moreover, the position of the white line peak of these catalysts shifted to low energy with increasing thermal-treatment temperature (Fig. S7, ESI<sup>†</sup>), suggesting that the valence state of V species decreased in this procedure. From the FT-EXAFS spectra (Fig. 3b), the peak located at around 1.6 Å was ascribed to the first V-O coordination shell.<sup>38</sup> Furthermore, the scattering peak due to the presence of the neighbouring V atoms (V-O-V) in the as-synthesized  $\text{VO}_x\text{-NbO}_y\text{@C}$  was hardly detected compared with  $\text{V}_2\text{O}_5$  or  $\text{VO}_2$ .<sup>39</sup> These results demonstrate that the vanadium species in the  $\text{VO}_x\text{-NbO}_y\text{@C}$  catalysts existed in the isolated monomeric  $\text{VO}_4$  state with tetrahedral coordination.

The catalytic performance of the  $\text{VO}_x\text{-NbO}_y\text{@C}$  was evaluated in the dehydrogenation of 1,2,3,4-tetrahydroquinoline. The commercial vanadium oxides showed low catalytic selectivity in this reaction (Table 1, entries 1 and 2). The nanorod-like niobium-based catalyst  $\text{NbO}_y\text{@C}$  gave 56.0% yield of quinoline. Compared with the  $\text{NbO}_y\text{@C}$  catalysts, incorporation of the vanadium species improved catalytic selectivity effectively, indicating a synergistic effect between vanadium oxide and niobium oxide. It is well known that the reducibility of vanadium in the redox mechanism is stronger than niobium.<sup>40</sup> The catalytic performance of the  $\text{VO}_x\text{-NbO}_y\text{@C}$  catalyst was significantly influenced by the thermal-treatment temperature.  $\text{VO}_x\text{-NbO}_y\text{@C-600}$  showed medium catalytic selectivity of the product. Quinoline

**Table 1** Catalytic performance of various materials in the dehydrogenation of 1,2,3,4-tetrahydroquinoline<sup>a</sup>

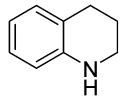
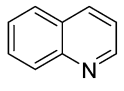
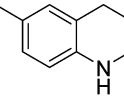
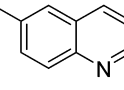
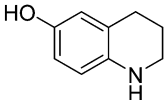
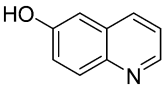
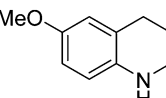
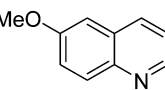
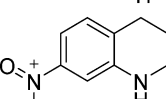
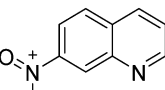
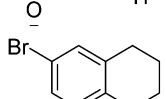
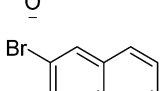
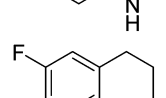
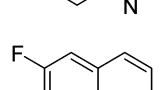
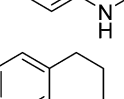
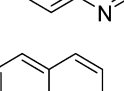
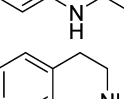
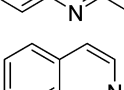
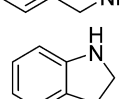
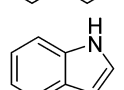
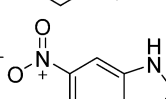
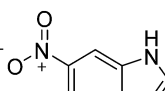
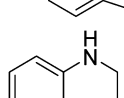
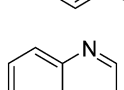
Entry <sup>a</sup>	Catalysts	Conv. <sup>b</sup> (%)	Sel. <sup>c</sup> (%)
1	V <sub>2</sub> O <sub>5</sub>	99	59.3
2	VO <sub>2</sub>	99	60.7
3	NbO <sub>y</sub> @C-800	99	56.0
4	VO <sub>x</sub> -NbO <sub>y</sub> @C-600	99	61.0
5	VO <sub>x</sub> -NbO <sub>y</sub> @C-700	99	79.2
6	VO <sub>x</sub> -NbO <sub>y</sub> @C-800	99	92.5

<sup>a</sup> Reaction conditions: 1,2,3,4-tetrahydroquinoline (0.5 mmol), catalyst (50 mg), DMSO (1.5 mL), H<sub>2</sub>O (0.5 mL), O<sub>2</sub> (0.5 MPa), 120 °C/16 h. <sup>b</sup> The yields were obtained by GC using chlorobenzene as the internal standard. <sup>c</sup> The other product was quinolinone.

yields increased with increasing thermal-treatment temperature (Table 1, entries 4–6). VO<sub>x</sub>-NbO<sub>y</sub>@C-800 achieved the highest catalytic performance with 92.5% yield of quinoline at full conversion of the substrate. As shown in Fig. 3c, the formal vanadium oxidation states deduced from the calibration curve decreased with increasing thermal-treatment temperature.<sup>41</sup> The increased proportion of low valent V species (Fig. 3c) may be the main reason for the improved selectivity of the catalyst treated at higher temperature. A small amount of quinolinone was detected owing to the over-oxidation reaction.<sup>42</sup> It has been reported that the V<sup>4+</sup> species in the mesoporous vanadia-titania nanoparticle (VTN) catalysts played a crucial role in the oxidative dehydrogenation of ethyl lactate to ethyl pyruvate.<sup>43</sup>

Reaction conditions were further optimized using VO<sub>x</sub>-NbO<sub>y</sub>@C-800, and the results are listed in the Tables S2 and S3 (ESI<sup>†</sup>). Solvents play a crucial role in this reaction. Organic solvents with weak polarity or moderate polarity, such as 1,3,5-trimethylbenzene, benzotrifluoride and dioxane, gave poor results. When polar solvents were used, quinoline was obtained in medium or good yield. These results could be related to the improved adsorption of the nonpolar reactant in the presence of polar solvents. The DMSO/H<sub>2</sub>O (v/v: 3/1) mixed solvent gave the best results. Furthermore, the scope of the reaction was explored under the optimized reaction conditions (Table 2). Tetrahydroquinoline derivatives bearing electron-donating groups (Table 2, entry 2) or electron-withdrawing groups (Table 2, entries 3 and 4) were catalytically transformed into the corresponding aromatic heterocycles in good to excellent yields. Apart from the tetrahydroquinoline derivatives, oxidative dehydrogenation of 1,2,3,4-tetrahydro-isoquinoline (Table 2, entry 5) and 1,2,3,4-tetrahydro-quinoxaline (Table 2, entry 8) also gave a high yield of the corresponding products. A moderate yield of indole was obtained in the case of indoline (Table 2, entry 6). While heterocycles were substituted with one strong electron withdrawing group like the NO<sub>2</sub> group, the desired yield of products could be obtained by increasing the oxygen pressure (Table 2, entries 3 and 7). These results indicate that electron-deficient aromatic rings retard adsorption or coordination of the substrates with the VO<sub>x</sub>-NbO<sub>y</sub>@C catalyst. It has been reported that electron-deficient groups usually impair the electron density of the aromatic ring which may lead to more difficult coordination of the substrates with the catalyst.<sup>44</sup> The yield of the reaction catalyzed

**Table 2** Dehydrogenation of N-heterocycles catalyzed by VO<sub>x</sub>-NbO<sub>y</sub>@C<sup>a</sup>

Ent.	Substrates	Products	Yield <sup>b</sup> (%)
1			92.5
2			93.6
3			65.9
4			53.9
5 <sup>c</sup>			87.3
6			78.8
7			61.9
8			74.2
9			89.8
10			62.1
11 <sup>c</sup>			86.4
12			79.9

<sup>a</sup> Reaction conditions: N-heterocycles (0.5 mmol), catalyst (50 mg), DMSO (1.5 mL), H<sub>2</sub>O (0.5 mL), O<sub>2</sub> (0.5 MPa), 120 °C/16 h. <sup>b</sup> Yields are for the isolated product. <sup>c</sup> O<sub>2</sub> (1.0 MPa).

by our V-based catalyst was among the highest reported in the literature (listed in the Table S4, ESI<sup>†</sup>), although the content of V in the catalyst was very low (0.07%), indicating that the monomeric VO<sub>x</sub> species were very efficient for promoting the reaction.

The recyclability of the VO<sub>x</sub>-NbO<sub>y</sub>@C catalyst was further investigated in the oxidative dehydrogenation of 1,2,3,4-tetrahydroquinoline. The used catalyst was recovered from the

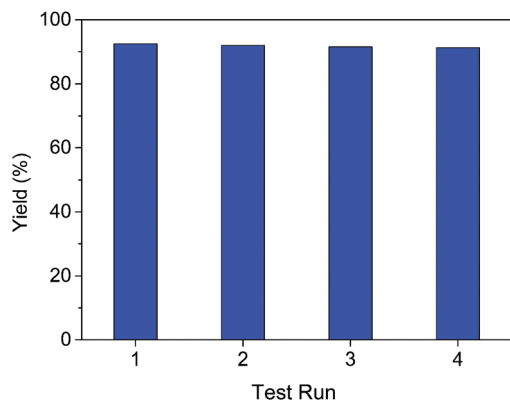


Fig. 4 Recyclability of  $\text{VO}_x\text{-NbO}_y\text{@C}$  in the oxidative dehydrogenation of 1,2,3,4-tetrahydroquinoline.

reaction mixture *via* simple centrifugation and reused in the next cycle after rinsing with DMSO. As shown in Fig. 4, the catalytic performance did not change notably after reusing four times, indicating an excellent catalytic stability of the catalyst. As shown in the XRD analysis of the reused  $\text{VO}_x\text{-NbO}_y\text{@C}$  catalyst (Fig. S8, ESI<sup>†</sup>), there is no significant change in the crystal phase structure of the reused catalyst compared with the fresh one. Moreover, the chemical composition of the catalyst, detected by XPS analysis, did not change obviously after reusing four times (Fig. S9, ESI<sup>†</sup>). Therefore, the  $\text{VO}_x\text{-NbO}_y\text{@C}$  catalyst displayed good recyclability in the reaction.

## Conclusions

In summary, the  $\text{VO}_x\text{-NbO}_y\text{@C}$  catalytic materials, in which the monomeric  $\text{VO}_x$  species were dispersed uniformly in the catalysts, was synthesized using a one-pot hydrothermal synthesis of the V/Nb inorganic/organic hybrid materials using the vanadium precursor, niobium tartrate and terephthalic acid followed by thermal treatment under a reducing atmosphere. The  $\text{VO}_x\text{-NbO}_y\text{@C}$  catalyst displayed excellent performance in the oxidative dehydrogenation of N-heterocycles. The monomeric  $\text{VO}_x$  species and the  $\text{NbO}_y$  in the composite catalytic materials showed a synergistic effect for promoting the reaction. The catalyst also exhibited good catalytic stability. We believe that the method used to prepare catalysts with monomeric  $\text{VO}_x$  species can also be used to design other effective catalysts.

## Conflicts of interest

There are no conflicts to declare.

## Acknowledgements

This work was financially supported by the National Key Research and Development Program of China (2017YFA0403003, 2017YFA0403103), the National Natural Science Foundation of China (21871277 and 21403248), and the Recruitment Program of

Global Youth Experts of China, and the Chinese Academy of Sciences (QYZDY-SSW-SLH013).

## Notes and references

- M. Mazidi, R. M. Behbahani and A. Fazeli, *Appl. Catal., B*, 2017, **209**, 190–202.
- M. J. Cheng and W. A. Goddard, *J. Am. Chem. Soc.*, 2013, **135**, 4600–4603.
- T. Lange, S. Heinrich, C. Liebner, H. Hieronymus and E. Klemma, *Chem. Eng. Sci.*, 2012, **69**, 440–448.
- A. Marberger, D. Ferri, M. Elsener and O. Krocher, *Angew. Chem., Int. Ed.*, 2016, **55**, 11989–11994.
- M. H. Zhu, J. K. Lai, U. Tumuluri, Z. L. Wu and I. E. Wachs, *J. Am. Chem. Soc.*, 2017, **139**, 15624–15627.
- Y. Zhou, Z. P. Ma, J. J. Tang, N. Yan, Y. H. Du, S. B. Xi, K. Wang, W. Zhang, H. M. Wen and J. Wang, *Nat. Commun.*, 2018, **9**, 2931.
- K. Kamata, T. Yamaura and N. Mizuno, *Angew. Chem., Int. Ed.*, 2012, **51**, 7275–7278.
- (a) J. J. H. B. Sattler, J. Ruiz-Martinez, E. Santillan-Jimenez and B. M. Weckhuysen, *Chem. Rev.*, 2014, **114**, 10613–10653; (b) X. Rozanska, R. Fortrie and J. Sauer, *J. Am. Chem. Soc.*, 2014, **136**, 7751–7761; (c) Z. J. Zhao, T. F. Wu, C. Y. Xiong, G. D. Sun, R. T. Mu, L. Zeng and J. L. Gong, *Angew. Chem., Int. Ed.*, 2018, **57**, 6791–6795; (d) U. Rodemerck, M. Stoyanova, E. V. Kondratenko and D. Linke, *J. Catal.*, 2017, **352**, 256–263.
- C. A. Carrero, R. Schloegl, I. E. Wachs and R. Schomaecker, *ACS Catal.*, 2014, **4**, 3357–3380.
- (a) S. Barman, N. Maity, K. Bhatte, S. Ould-Chikh, O. Dachwald, C. Haessner, Y. Saih, E. Abou-Hamad, I. Llorens, J. L. Hazemann, K. Kohler, V. D'Elia and J. M. Basset, *ACS Catal.*, 2016, **6**, 5908–5921; (b) U. Rodemerck, M. Stoyanova, E. V. Kondratenko and D. Linke, *J. Catal.*, 2017, **352**, 256–263.
- B. Schimmoeller, Y. J. Jiang, S. E. Pratsinis and A. Baiker, *J. Catal.*, 2010, **274**, 64–75.
- B. Mitra, I. E. Wachs and G. Deo, *J. Catal.*, 2006, **240**, 151–159.
- (a) B. T. Qiao, A. Q. Wang, X. F. Yang, L. F. Allard, Z. Jiang, Y. T. Cui, J. Y. Liu, J. Li and T. Zhang, *Nat. Chem.*, 2011, **3**, 634–641; (b) E. J. Peterson, A. T. DeLaRiva, S. Lin, R. S. Johnson, H. Guo, J. T. Miller, J. H. Kwak, C. H. F. Peden, B. Kiefer, L. F. Allard, F. H. Ribeiro and A. K. Datye, *Nat. Commun.*, 2014, **5**, 4885; (c) P. X. Liu, Y. Zhao, R. X. Qin, S. G. Mo, G. X. Chen, L. Gu, D. M. Chevrier, P. Zhang, Q. Guo, D. D. Zang, B. H. Wu, G. Fu and N. F. Zheng, *Science*, 2016, **352**, 797–801; (d) L. Nie, D. H. Mei, H. F. Xiong, B. Peng, Z. B. Ren, X. I. P. Hernandez, A. DeLaRiva, M. Wang, M. H. Engelhard, L. Kovarik, A. K. Datye and Y. Wang, *Science*, 2017, **358**, 1419–1423; (e) Y. J. Chen, S. F. Ji, W. M. Sun, W. X. Chen, J. C. Dong, J. F. Wen, J. Zhang, Z. Li, L. R. Zheng, C. Chen, Q. Peng, D. S. Wang and Y. D. Li, *J. Am. Chem. Soc.*, 2018, **140**, 7407–7410; (f) B. Zhang,

- H. Asakura, J. Zhang, J. G. Zhang, S. De and N. Yan, *Angew. Chem., Int. Ed.*, 2016, **55**, 8319–8323.
- 14 X. J. Wang, X. Zhang, P. Li, K. Otake, Y. X. Cui, J. F. Lyu, M. D. Krzyaniak, Y. Y. Zhang, Z. Y. Li, J. Liu, C. T. Buru, T. Islamoglu, M. R. Wasielewski, Z. Li and O. K. Farha, *J. Am. Chem. Soc.*, 2019, **141**, 8306–8314.
- 15 X. F. Yang, A. Q. Wang, B. T. Qiao, J. Li, J. Y. Liu and T. Zhang, *Acc. Chem. Res.*, 2013, **46**, 1740–1748.
- 16 (a) T. Zhang, D. Zhang, X. H. Han, T. Dong, X. W. Guo, C. S. Song, R. Si, W. Liu, Y. F. Liu and Z. K. Zhao, *J. Am. Chem. Soc.*, 2018, **140**, 16936–16940; (b) S. B. Tian, Z. Y. Wang, W. B. Gong, W. X. Chen, Q. C. Feng, Q. Xu, C. Chen, C. Chen, Q. Peng, L. Gu, H. J. Zhao, P. Hu, D. S. Wang and Y. D. Li, *J. Am. Chem. Soc.*, 2018, **140**, 11161–11164.
- 17 (a) T. B. Li, F. Liu, Y. Tang, L. Li, S. Miao, Y. Su, J. Y. Zhang, J. H. Huang, H. Sun, M. Haruta, A. Q. Wang, B. T. Qiao, J. Li and T. Zhang, *Angew. Chem., Int. Ed.*, 2018, **57**, 7795–7799; (b) J. W. Wan, W. X. Chen, C. Y. Jia, L. R. Zheng, J. C. Dong, X. S. Zheng, Y. Wang, W. S. Yan, C. Chen, Q. Peng, D. S. Wang and Y. D. Li, *Adv. Mater.*, 2018, **30**, 1705369.
- 18 G. L. Liu, A. W. Robertson, M. M. J. Li, W. C. H. Kuo, M. T. Darby, M. H. Muhieddine, Y. C. Lin, K. Suenaga, M. Stamatakis, J. H. Warner and S. C. E. Tsang, *Nat. Chem.*, 2017, **9**, 810–816.
- 19 L. Tsetseris, N. Kalfagiannis, S. Logothetidis and S. T. Pantelides, *Phys. Rev. Lett.*, 2007, **99**, 125503.
- 20 L. Jiao, G. Wan, R. Zhang, H. Zhou, S. H. Yu and H. L. Jiang, *Angew. Chem., Int. Ed.*, 2018, **57**, 8525–8529.
- 21 (a) V. Sridharan, P. A. Suryavanshi and J. C. Menendez, *Chem. Rev.*, 2011, **111**, 7157–7259; (b) E. Vitaku, D. T. Smith and J. T. Njardarson, *J. Med. Chem.*, 2014, **57**, 10257–10274.
- 22 (a) D. V. Jawale, E. Gravel, N. Shah, V. Dauvois, H. Y. Li, I. N. N. Namboothiri and E. Doris, *Chem. – Eur. J.*, 2015, **21**, 7039–7042; (b) C. Deraedt, R. Ye, W. T. Ralston, F. D. Toste and G. K. Somorjai, *J. Am. Chem. Soc.*, 2017, **139**, 18084–18092.
- 23 (a) Y. H. Han, Z. Y. Wang, R. R. Xu, W. Zhang, W. X. Chen, L. R. Zheng, J. Zhang, J. Luo, K. L. Wu, Y. Q. Zhu, C. Chen, Q. Peng, Q. Liu, P. Hu, D. S. Wang and Y. D. Li, *Angew. Chem., Int. Ed.*, 2018, **57**, 11262–11266; (b) G. Jaiswal, M. Subaramanian, M. K. Sahoo and E. Balaraman, *ChemCatChem*, 2019, **11**, 2449–2457.
- 24 G. Jaiswal, V. G. Landge, D. Jagadeesan and E. Balaraman, *Nat. Commun.*, 2017, **8**, 2147.
- 25 P. Ryabchuk, A. Agapova, C. Kreyenschulte, H. Lund, H. Junge, K. Junge and M. Beller, *Chem. Commun.*, 2019, **55**, 4969–4972.
- 26 N. Zumbregel, M. Sako, S. Takizawa, H. Sasai and H. Groger, *Org. Lett.*, 2018, **20**, 4723–4727.
- 27 M. Karki, H. C. Araujo and J. Magolan, *Synlett*, 2013, 1675–1678.
- 28 (a) K. Tanabe and S. Okazaki, *Appl. Catal., A*, 1995, **133**, 191–218; (b) I. Nowak and M. Ziolek, *Chem. Rev.*, 1999, **99**, 3603–3624; (c) P. Carniti, A. Gervasini, C. Tiozzo and M. Guidotti, *ACS Catal.*, 2014, **4**, 469–479.
- 29 (a) A. Qiao, V. N. Kalevaru, J. Radnik, A. S. Kumar, N. Lingaiah, P. S. S. Prasad and A. Martin, *Catal. Commun.*, 2013, **30**, 45–50; (b) M. Sarzi-Amade, S. Morselli, P. Moggi, A. Maione, P. Ruiz and M. Devillers, *Appl. Catal., A*, 2005, **284**, 11–20; (c) N. Ballarini, F. Cavana, C. Cortelli, C. Giunchi, P. Nobili, F. Trifirò, R. Catani and U. Cornaro, *Catal. Today*, 2003, **78**, 353–364.
- 30 (a) M. Ziolek, A. Lewandowska, B. Grzybowska and A. Klisinska, *React. Kinet. Catal. Lett.*, 2003, **80**, 199–206; (b) B. Kilos, M. Aouine, I. Nowak, M. Ziolek and J. C. Volta, *J. Catal.*, 2004, **224**, 314–325; (c) R. R. Langeslay, D. M. Kaphan, C. L. Marshall, P. C. Stair, A. P. Sattelberger and M. Delferro, *Chem. Rev.*, 2019, **119**, 2128–2191.
- 31 A. Sarkar and P. Pramanik, *Microporous Mesoporous Mater.*, 2009, **117**, 580–585.
- 32 (a) J. S. Xu, J. X. Zhu, X. F. Yang, S. W. Cao, J. G. Yu, M. Shalom and M. Antonietti, *Adv. Mater.*, 2016, **28**, 6727; (b) W. Kicinski and A. Dziura, *Carbon*, 2014, **75**, 56–67.
- 33 J. Sun, W. Sun, L. Du, C. Du, Y. Gao and G. Yin, *Fuel Cells*, 2018, **18**, 360–368.
- 34 (a) W. Q. Wu, K. L. Ding, J. Liu, T. Drake, P. Stair and E. Weitz, *J. Phys. Chem. C*, 2017, **121**, 26794–26805; (b) Y. L. Meng, T. Wan, S. Chen, Y. J. Zhao, X. B. Ma and J. L. Gong, *Appl. Catal., B*, 2014, **160**, 161–172; (c) V. V. Kaichev, G. Y. Popova, Y. A. Chesalov, A. A. Saraev, D. Y. Zemlyanov, S. A. Beloshapkin, A. Knop-Gericke, R. Schlögl, T. V. Andrushkevich and V. I. Bukhtiyarov, *J. Catal.*, 2014, **311**, 59–70.
- 35 (a) E. N. Alvar, B. Zhou and S. H. Eichhorn, *J. Mater. Chem. A*, 2016, **4**, 6540–6552; (b) C. W. Lin, A. Posadas, T. Hadamek and A. A. Demkov, *Phys. Rev. B: Condens. Matter Mater. Phys.*, 2015, **92**, 035110.
- 36 C. J. Patridge, L. Whittaker, B. Ravel and S. Banerjee, *J. Phys. Chem. C*, 2012, **116**, 3728–3736.
- 37 T. Mitsudome, K. Miyagawa, Z. Maeno, T. Mizugaki, K. Jitsukawa, J. Yamasaki, Y. Kitagawa and K. Kaneda, *Angew. Chem., Int. Ed.*, 2017, **56**, 9381–9385.
- 38 Y. F. Wu, L. L. Fan, Q. H. Liu, S. Chen, W. F. Huang, F. H. Chen, G. M. Liao, C. W. Zou and Z. Y. Wu, *Sci. Rep.*, 2015, **5**, 9328.
- 39 K. Kaneda, T. Hara, N. Hashimoto, T. Mitsudome, T. Mizugaki and K. Jitsukawa, *Catal. Today*, 2010, **152**, 93–98.
- 40 M. Ziolek, *Catal. Today*, 2003, **78**, 47–64.
- 41 C. J. Patridge, C. Jaye, T. A. Abteu, B. Ravel, D. A. Fischer, A. C. Marschilok, P. H. Zhang, K. J. Takeuchi, E. S. Takeuchi and S. Banerjee, *J. Phys. Chem. C*, 2011, **115**, 14437–14447.
- 42 X. J. Cui, Y. H. Li, S. Bachmann, M. Scalone, A. E. Surkus, K. Junge, C. Topf and M. Beller, *J. Am. Chem. Soc.*, 2015, **137**, 10652–10658.
- 43 W. Zhang, G. Innocenti, P. Oulego, V. Gitis, H. H. Wu, B. Ensing, F. Cavani, G. Rothenberg and N. R. Shiju, *ACS Catal.*, 2018, **8**, 2365–2374.
- 44 P. Preuster, C. Papp and P. Wasserscheid, *Acc. Chem. Res.*, 2017, **50**, 74–85.